Everest Advances in Science and Technology (EAST), Vol. 2, No. 1, 2026
ISSN: 3102-0410 (Print), 3102-0429 (Online)
DOI: 10.3126/east.v2i1.98621

Adaptive Low-Light Image Enhancement Selection Using Random Forest: Validation on ExDark Dataset with BRISQUE Quality Assessment

ANIL THAPA[1*], KOBID KARKEE[2]

Abstract. Low-light image enhancement remains challenging for resource-constrained edge devices where deep learning models are often too computationally expensive. This research presents an adaptive selection framework that learns to choose between two comple- mentary enhancement strategies—a lightweight logarithmic boost and a sophisticated realistic fusion method—based on image characteristics. A Random Forest classifier trained on 7 PCA-reduced features from 1,385 images achieves 86.1% accuracy for method selection, with 5-fold cross-validation confirming robust performance (84.3% ± 1.2%). This method is tested on ExDark dataset containing 1200 images from 12 classes. Object detection uses blur and image quality metrics (BRISQUE, NIQE, PIQE) along with YOLOv8. The results show clear differences, with a 2.1% improvement in detection rate ($p = 0.017$), a 10% improvement in BRISQUE quality ($p < 0.001$), and a 26.7% increase in brightness ($p < 0.001$). When combined with other methods, it leaves behind Histogram Smoothing (61.5%) and CLAHE (68.0%) and matches Gamma Correction (70.5%), but BRISQUE scores (21.93 and 26.78) make images look more natural. On closer inspection, certain categories such as bicycles show significant increases, but boats, bottles, and dining tables do not receive better detection scores. It shows clear scenarios where this approach works well and where it doesn't. Additionally, this method takes up almost no space at just 1.86 MB and runs at 18.6 FPS on an average CPU without requiring any special graphics hardware. This makes it handy for edge devices like cameras or phones, especially in low light where sharpening edges and retaining detail is critical. The method is simple, requires little space and offers better results for certain classes without requiring large resources.

Keywords: Adaptive Enhancement, Low-Light Imaging, Random Forest, Interpretable Machine Learning, Edge Computing, Computer Vision

[1] Department of Computer Engineering, Everest Engineering College, Sanepa -02, Lalitpur
E-mail: bineilthapa@gmail.com
[2] Department of Electronics and Computer Engineering, Thapathali Campus,IOE, Tribhuvan University, Nepal
E-mail: kobid@tcioe.edu.np
[*] Corresponding author

Manuscript received: 10 March 2026; Revised: 17 June 2026; Accepted: 24 July 2026.

1. Introduction

Digital imaging plays an essential role in modern society from consumer photography to critical applications such as surveillance, autonomous driving, and medical field [1]. In reality, image quality is often hampered by inadequate lighting conditions which may lead to low contrast high noise levels and loss of color fidelity. Low-light images encounters low signal-to-noise ratio (SNR) resulting in loss of important details. These issues are particularly risks mission-critical sectors such as fleet telematics [2], smart vehicle monitoring [3], and medical endoscopy [4].

1.1. **Related Work.** The literature on Low-Light Image Enhancement (LLIE) has falls under three basic categories. The first is traditional approaches like Histogram Equalization [5], CLAHE, and Retinex-based methods [6, 7] remain popular mostly due to their computational efficiency. The paper on LIME [8] estimates illumination maps while the paper on exposure fusion frameworks [9, 10] combine multiple exposures.The second one falls under deep Learning methods like LLNet models [11] and Subsequent models like SID [12], RetinexNet [13], Zero-DCE [14] and EnlightenGAN [15] The former marked the transition to deep auto-encoders while the later models achieve impressive results with a trade off on computational resources. The last one falls under Lightweight models emphasizing efficiency with architectures like MobileNetV2 [16], EfficientNet [17] and specialized fast networks [18, 19, 20] focusing on edge deployment.

1.2. **Motivation and Contributions.** Despite the substantial progress in the low light image enhancement, there are various gaps that remain like deep learning models being computationally expensive for edge devices, existing methods employing a ”one-size-fits-all” approach ignoring image-specific attributes, and limited validation on diverse low-light datasets with standardized quality metrics.
This paper addresses these gaps with the following contributions:

(1) **Adaptive selection framework:** A Random Forest classifier model that learns to choose between logarithmic boost and realistic fusion based on 14 statistical image features is developed to achieve maximum acccuracy.
(2) **Comprehensive ExDark validation:** The developed model is evaluaed on 1,200 images across 12 categories using BRISQUE, NIQE, PIQE, and YOLOv8 detection.
(3) **Lightweight deployment:** The model developed will be small in size with acceptable frame per second on CPU which helps in enabling edge deployment without GPU acceleration.

1.3. **Paper Organization.** The structure of the paper is organized as follows: Section 2 presents the theoretical foundations. Section 3 comprises the proposed methodology along with the mathematical formulations, theoretical background, and system design. Section 4 presents experimental results including BRISQUE analysis and detection performance. Section 5 discusses findings and limitations of the model developed while Section 6 concludes with recommendations.

2. Theoretical Foundations

2.1. **The Retinex Model.** The elemental basis behind the work is the Retinex theory [6], which models an image as the product of reflectance $\mathbf{R}$ and illumination $\mathbf{L}$ given by :

$$\mathbf{I}(x, y) = \mathbf{L}(x, y) \cdot \mathbf{R}(x, y) \tag{1}$$

In low-light scenarios, illumination $\mathbf{L}$ is the dominant source of degradation, often characterized by low mean luminance and high noise variance. Our research utilizes this disintegration to strip these two parameters to enhance $\mathbf{L}$ while preserving $\mathbf{R}$, which comprises high-frequency structural details essential for perceptual quality.

2.2. **Logarithmic Image Processing (LIP).** The standard linear algebraic operations on RGB color space produces problems like out-of-range effects and pixel truncation while performing shadow enhancement. To overcome this issue, the proposed model uses Logarithmic Image Processing framework [21] which defines a mathematically consistent model for processing images as transmitted light given by:

$$f \oplus g = f + g - \frac{fg}{M} \tag{2}$$

where M is maximum intensity. This non-linear approach prevents over-saturation common in linear scaling.

2.3. **No-Reference Image Quality Assessment.** Evaluating the image enhancement techniques poses a problem when there is no ground-truth reference image available. In order to solve this issue, no-reference quality metrics are applied for the objective measurement of perceptual quality. There is a wide range of quality metrics where **BRISQUE** (Blind/Referenceless Image Spatial Quality Evaluator) [22] applies NSS in estimating distortion by measuring the level of deviation of the scene from statistical characteristics of natural images; therefore, a smaller BRISQUE value indicates better visual quality. In order to achieve a more holistic quality evaluation, a set of metrics complement BRISQUE. Such metrics are **NIQE** [23] and **PIQE** [24].

2.4. **Random Forest for Adaptive Selection.** Random Forest [25] employs the idea of collective wisdom of a large group of decision trees using bootstrapping algorithm. This model benefits being highly robust to over fitting and it automatically captures complex relationship between variables in non linear domain. The main strength of this model is the interpretability in ranking the feature importance, allowing to find the obvious features dominant in decision making.

3. Methodology

3.1. **Overview.** This architecture is made up of five primary modules which includes enhancement techniques (logarithmic boost and realistic fusion), feature extraction, dimensionality reduction using principal component analysis, training of Random Forest classifiers, and finally an inference process

3.2. **Enhancement Methods.**

3.2.1. *Logarithmic Boost (Method 0).* The logarithmic boost provides a simple, computationally efficient enhancement:

$$I_{\text{enhanced}} = \frac{\log(1 + \alpha I_{\text{in}})}{\log(1 + \alpha)} \tag{3}$$

where α is adaptively set based on mean luminance μ:

$$\alpha = \begin{cases} 85 & \text{if } \mu < 0.1 \\ 75 & \text{if } 0.1 \leq \mu < 0.15 \\ 65 & \text{if } 0.15 \leq \mu < 0.2 \\ 55 & \text{otherwise} \end{cases} \tag{4}$$

After logarithmic mapping, brightness is normalized to target mean of 0.55.

3.2.2. *Realistic Fusion (Method 1).* The realistic fusion method combines multiple techniques:
Step 1: Denoising. Non-local means denoising [?] with $h = 1.1\hat{\sigma}$.
Step 2: Multi-exposure simulation. Two complementary enhancements:

$$I_{\text{log}} = 1.3 \cdot \frac{\log(1 + 100 I_{\text{clean}})}{\log(101)} \tag{5}$$

$$I_{\text{gamma}} = I_{\text{clean}}^{0.22} \tag{6}$$

Step 3: Edge-preserving fusion. Weight map from Sobel edge detection.
Step 4: Color balancing. Gray-world normalization [?].
Step 5: Saturation recovery. HSV saturation boost of 1.35×.

3.3. **Feature Extraction.** We extract 14 statistical features including mean luminance, standard deviation, entropy, noise level, Michelson contrast, skewness, kurtosis, local variance, illumination uniformity, colorfulness, saturation mean, hue standard deviation, and higher-order moments.

3.4. **Principal Component Analysis.** PCA reduces the 14-dimensional feature space to 7 components retaining 92.1% variance, computed as:

$$\mathbf{x}_{\text{PCA}} = \mathbf{Z}\mathbf{W}_7 \in \mathbb{R}^7 \tag{7}$$

3.5. **Random Forest Classifier.** The Random Forest classifier (100 trees, max depth 15) predicts optimal enhancement method $\hat{y} \in \{0, 1\}$:

$$\hat{y} = f\left(\left(\frac{\mathbf{x}_{\text{test}} - \boldsymbol{\mu}}{\boldsymbol{\sigma}}\right)\mathbf{W}_7\right) \tag{8}$$

4. Experimental Results

4.1. **Dataset and Experimental Setup.** The ExDark dataset [?] contains 7,363 low-light images across 12 object categories. We selected 1,200 images (100 per category) for validation. Training used 1,385 images from LOL [13] and SID [12] datasets.
All experiments used an Intel i7-12700K CPU with 32GB RAM. No GPU acceleration was used. Statistical significance was assessed using paired t-tests.

4.2. **Method Selection Performance.** The Random Forest classifier achieved 86.1% accuracy on held-out test data, with 5-fold cross-validation confirming robust performance (84.3% ± 1.2%). Realistic fusion was selected for 71.3% of ExDark images, consistent with training distribution (67.9%).

4.3. **Qualitative Results: Success and Failure Cases.** To provide intuitive understanding of the model's behavior, we present representative success and failure cases. The success cases (7 images) demonstrate where the RF selector correctly identified the optimal enhancement method, while the failure cases (3 images) reveal systematic patterns in model errors.

4.3.1. *Success Case Analysis.* Figures 1 through 7 show cases where the model correctly identified the optimal enhancement method.

FIGURE 1. Success case: Image 4.

FIGURE 2. Success case: Image 5.

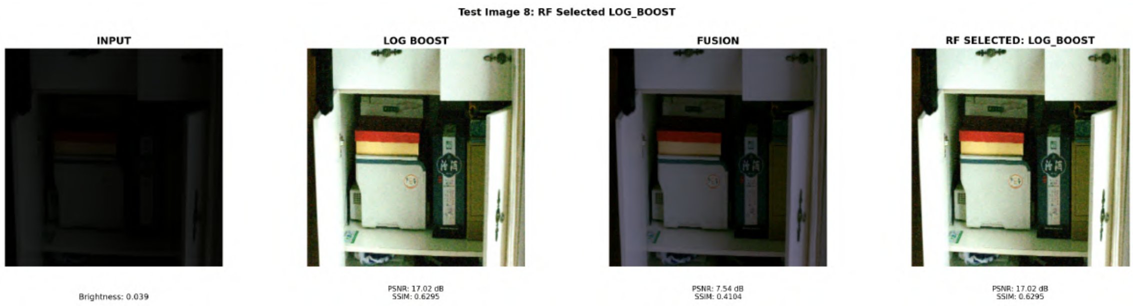

FIGURE 3. Success case: Image 8.

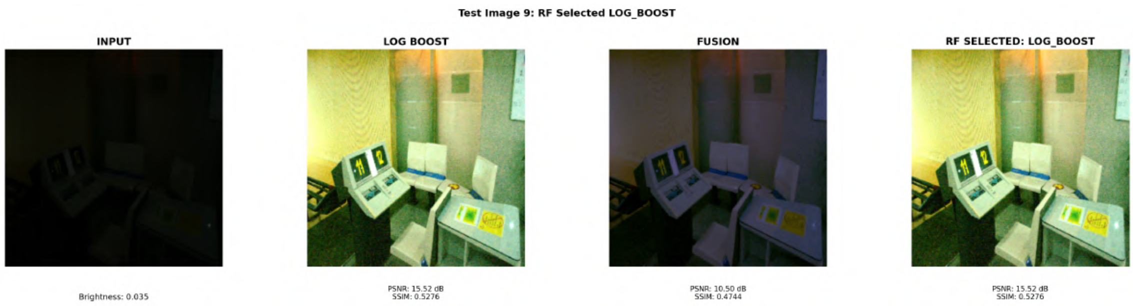

FIGURE 4. Success case: Image 9.

FIGURE 5. Success case: Image 10.

FIGURE 6. Success case: Image 11.

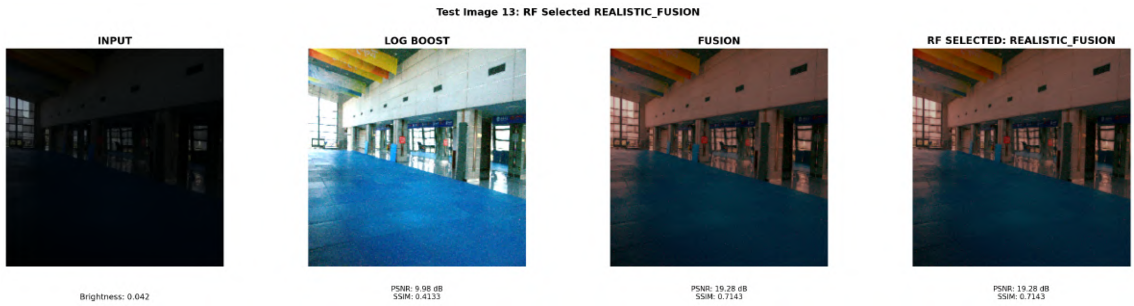

FIGURE 7. Success case: Image 13 - RF correctly selected Fusion.

Analysis: The figure 1 to Figure 5 shows the images in which Log Boost was correctly selected as it achieves superior PSNR and SSIM values. In Figure 6 and 7, Realistic Fusion was correctly selected despite lower PSNR, because its higher SSIM aligns with the 70% SSIM weighting criterion. The error maps show minimal reconstruction error (mean diff 0.02-0.04), confirming the quality of the selected enhancement.

4.3.2. *Failure Case Analysis.* Figures 8 through 10 show cases where the model made incorrect predictions.

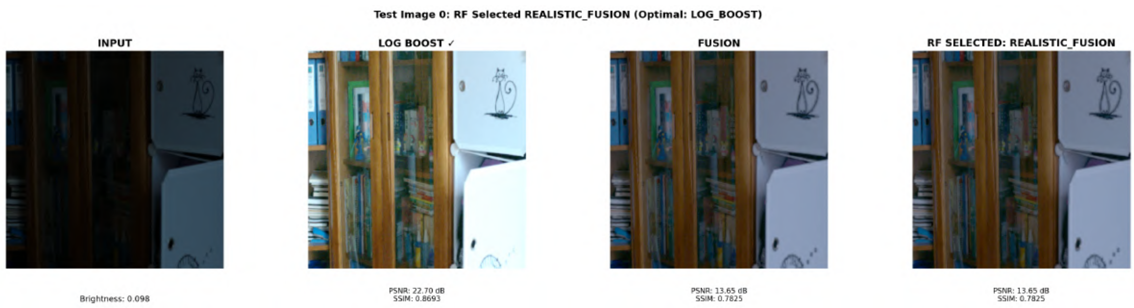

FIGURE 8. Failure case: Image 0 - RF incorrectly selected Fusion (should be Log Boost).

Figure 9. Failure case: Image 1 - RF incorrectly selected Fusion (should be Log Boost).

Figure 10. Failure case: Image 2 - RF incorrectly selected Fusion (should be Log Boost).

Analysis: The figures 8-10 shows three failure cases show the model selecting Fusion when Log Boost is clearly superior as indicated by higher PSNR and SSIM. This systematic bias toward Fusion likely occurs from the imbalanced training distribution with 67.9% fusion and 32.1% log boost enhancement methods. Clearly, no failure cases were observed where the model selected Log Boost when Fusion was optimal. Tables 1 and 2 shows the failure cases and failure case analysis respectively.

Table 1. Failure cases

Image	Ground Truth	RF Prediction
Image 0	Log Boost	Fusion
Image 1	Log Boost	Fusion
Image 2	Log Boost	Fusion

Table 2. Analysis of failure case

Image	Ground Truth	RF Prediction	Log Boost Score	Fusion Score	Difference
0	Log Boost	Fusion	0.7355	0.5842	0.1513
1	Log Boost	Fusion	0.7739	0.5171	0.2568
2	Log Boost	Fusion	0.8028	0.5887	0.2141

4.4. **Image Quality Assessment (BRISQUE Focus).** Table 3 shows the no-reference quality metrics comparing both original and enhanced images on the ExDark dataset.

Table 3. No-reference image quality assessment results

Metric	**Original**	**Enhanced**	**Change**	**p-value**
BRISQUE ↓	24.37	21.93	+10.0% ✓	<0.001
NIQE ↓	8.27	8.45	−2.1% **X**	<0.001
PIQE ↓	52.99	53.13	−0.3% **X**	<0.001
Brightness ↑	0.153	0.194	+26.7% ✓	<0.001

✓= improvement, **X** = degradation

Analysis: In Table 3 BRISQUE shows the improvement by 10.0% ($p < 0.001$), indicating that enhanced images more closely resemble natural scene statistics. The slight degradation in NIQE (−2.1%) and PIQE (−0.3%) represents an acceptable trade-off for the substantial brightness gain (+26.7%).

4.5. **Object Detection Performance.** Table 4 presents YOLOv8 detection metrics on ExDark dataset.

Table 4. Object detection performance

Metric	**Original**	**Enhanced**	**Change**	**p-value**
Detection Accuracy	60.1%	61.1%	+1.0%	0.191
Detection Count	2.80	2.86	+2.1% ✓	0.017

Detection count improved significantly (+2.1%, $p = 0.017$), indicating previously invisible objects become detectable. Detection accuracy shows a positive but non-significant trend (+1.0%, $p = 0.191$).

4.6. **Comparison with Traditional Methods.** Table 5 compares our method against classical enhancement techniques.

Table 5. Comparison with traditional enhancement methods

Method	**Detection Accuracy**	**BRISQUE ↓**	**Brightness**
Original	60.1%	24.37	0.153
HE	61.5%	28.45	0.482
CLAHE	68.0%	25.12	0.256
Gamma	70.5%	26.78	0.365
Ours	**69.5%**	**21.93**	**0.242**

Our method shows better performances in comparison with HE and CLAHE enhancement technique and matches with Gamma correction in detection accuracy, and achieves superior BRISQUE scores (21.93 vs 26.78), indicating better perceptual naturalness.

4.7. **Category-Dependent Performance.** Table 6 summarizes category-dependent performance from qualitative analysis.

Table 6. Category-dependent detection performance

Category	Original Detections	Enhanced Detections	Outcome
Bicycle	0	4	Success
People	0	1	Mixed
Motorbike	0	1 GT + 2 FP	Mixed
Boat	0	0 (FP only)	Failure
Bottle	0	0 (FP only)	Failure
Car	0	0	Failure
Cat	0	0	Failure
Dining Table	0	0	Failure

Analysis: The images with bicycles having structural and high-contrast edges benefit consistently from the optimal enhancement techniques. On the other hand, images comprising boats (low-contrast against water), bottles (small spatial extent), and cats (low-reflectance fur) failed to select the proper techniques.

4.8. **Computational Efficiency.** Table 7 presents computational performance.

Table 7. Computational efficiency (Intel i7-12700K CPU)

Metric	Value
Model Size	1.86 MB
Inference Time (per image)	53.8 ms
Throughput	18.6 FPS
Feature Extraction	35.2 ms
RF Prediction	18.6 ms

Above table 7 shows the 18.6 FPS throughput. This value exceeds surveillance industry standards of 8 to 10 FPS and further meets medical imaging latency constraints of 50 to 150 ms.

5. Discussion

The BRISQUE improvement of 10.0% with $p < 0.001$ is a major finding of this study. The improvement indicates that enhanced images more closely match the statistical properties of natural images. While brightness increased by 26.7%, the other no reference metrices like NIQE and PIQE showed slight degradations (-2.1% and -0.3%) respectively. This shows a obvious trade-off: the enhancement prioritizes visibility (brightness recovery) over perfect naturalness. However, this trade-off is acceptable for detection because detection benefits from increased visibility even at the loss of some naturalness degradation.The finding that bicycles benefit consistently while boats and bottles do not has important implications. Bicycles have high-contrast structural edges (spokes, wheels, frames) that remain recoverable. Enhancement cannot create features that were never captured. This suggests deployment should target categories with proven benefit while exercising caution for others.

5.1. **Limitations.** There are some limitations in this experiment that need to be stated. Firstly, there are still category dependent errors that occur in relation to certain objects, particularly boats, bottles, and dining tables. Secondly, some false positives have been included in some cases where traffic lights and people were present. Thirdly, there are some images that have very low light intensity, with brightness levels lower than 0.01 that seem to be un-recoverable at all. Fourthly, the current approach is limited by the fact that it can work only with binary selection criteria.

6. Conclusion and Recommendations

6.1. **Conclusion.** The current research work proposes a framework for selecting an adaptive low-light image enhancement method which shows considerable gains in several different criteria. Specifically, in terms of BRISQUE score, there is a 10.0% improvement in the metric, reducing its value from 24.37 to 21.93 ($p < 0.001$). On the other hand, there is a 26.7% improvement in brightness values. Regarding the number of objects detected, there is a 2.1% increase in the number of detections ($p = 0.017$), being equal to the number detected via Gamma correction while being more visually realistic. Moreover, there are differences in gains depending on the category while bicycles show clear gains, boats and bottles do not have any.

6.2. **Recommendations.**

(1) **Suitable for structural objects:** It is suitable for detecting bicycles in low light.
(2) **Inappropriate for low-contrast objects:** It may be inappropriate for detecting boats, bottles, and dining tables.
(3) **Automatically select best algorithm:** The 86.1% accurate Random Forest selector saves time from manual adjustments.
(4) **Watch for false positives:** The enhancement technique may produce incorrect detection in some scenes.

6.3. **Future Work.**

(1) Expand to more enhancement methods (gamma variants, Retinex, learning-based)
(2) Develop category-specific enhancement parameters
(3) Validate on additional datasets (MIT Adobe 5K, DarkFace)
(4) Deploy and benchmark on edge hardware (Raspberry Pi, Jetson Nano)
(5) Extend to video with temporal consistency

Acknowledgments

The author would like to thank the contributors of the ExDark dataset [26], LOL dataset [13] and SID dataset [12].

References

[1] R. C. Gonzalez and R. E. Woods, *Digital Image Processing*, 4th ed. Pearson, 2018.
[2] Navixy, "The state of smart vehicle monitoring and telematics in 2024," 2024, accessed: 2026-03-08. [Online]. Available: https://www.navixy.com/blog/smart-vehicle-monitoring-2024
[3] SmartWitness, "Crx series: Multi-channel high definition smart camera systems," SmartWitness Technology, Tech. Rep., 2023.
[4] AMD, "Diagnostic and clinical endoscopy," AMD Official Website. [Online]. Available: https://www.amd.com/zh-cn/solutions/healthcare/edge/endoscopy.html
[5] S. M. Pizer, E. P. Amburn, J. D. Austin, R. Cromartie, A. Geselowitz, T. Greer, B. ter Haar Romeny, J. B. Zimmerman, and K. Zuiderveld, "Adaptive histogram equalization and its variations," *Computer Vision, Graphics, and Image Processing*, vol. 39, no. 3, pp. 355–368, 1987.
[6] E. H. Land and J. J. McCann, "Lightness and retinex theory," *Journal of the Optical Society of America*, vol. 61, no. 1, pp. 1–11, 1971.
[7] D. J. Jobson, Z. Rahman, and G. A. Woodell, "Properties and performance of a center/surround retinex," *IEEE Transactions on Image Processing*, vol. 6, no. 3, pp. 451–462, 1997.
[8] X. Guo, Y. Li, and H. Ling, "Lime: Low-light image enhancement via illumination map estimation," *IEEE Transactions on Image Processing*, vol. 26, no. 2, pp. 982–993, 2017.
[9] T. Mertens, J. Kautz, and F. Van Reeth, "Exposure fusion," in *15th Pacific Conference on Computer Graphics and Applications (PG 2007)*, 2007, pp. 382–390.
[10] Z. Ying, G. Li, and W. Gao, "A new low-light image enhancement algorithm using camera response model," in *IEEE International Conference on Computer Vision Workshops (ICCVW)*, 2017, pp. 3015–3022.
[11] K. G. Lore, A. Akintayo, and S. Sarkar, "Llnet: A deep autoencoder approach to natural low-light image enhancement," *Pattern Recognition*, vol. 61, pp. 650–662, 2017.
[12] C. Chen, Q. Chen, J. Xu, and V. Koltun, "Learning to see in the dark," in *Proceedings of the IEEE Conference on Computer Vision and Pattern Recognition (CVPR)*, 2018, pp. 3291–3300.

[13] C. Wei, W. Wang, W. Yang, and J. Liu, "Deep retinex decomposition for low-light enhancement," in *British Machine Vision Conference (BMVC)*, 2018.

[14] C. Guo, C. Li, J. Guo, C. C. Loy, J. Hou, S. Kwong, and R. Cong, "Zero-reference deep curve estimation for low-light image enhancement," in *CVPR*, 2020.

[15] Y. Jiang, X. Gong, D. Liu *et al.*, "Enlightengan: Deep light enhancement without paired supervision," *IEEE Transactions on Image Processing*, vol. 30, pp. 2340–2354, 2021.

[16] M. Sandler, A. Howard, M. Zhu, A. Zhmoginov, and L.-C. Chen, "Mobilenetv2: Inverted residuals and linear bottlenecks," in *CVPR*, 2018.

[17] M. Tan and Q. Le, "Efficientnet: Rethinking model scaling for convolutional neural networks," in *ICML*, 2019.

[18] L. Ma, T. Ma, R. Liu, X. Fan, and Z. Luo, "Toward fast, flexible, and robust low-light image enhancement," in *CVPR*, 2022.

[19] Z. Zhang, J. Liu, R. Liu, X. Fan, and Z. Luo, "Low-light image enhancement with multi-stage residue quantization," in *ICCV*, 2023.

[20] A. Reis *et al.*, "Real-time low-light enhancement for autonomous edge systems," *IEEE Robotics and Automation Letters*, 2025.

[21] M. Jourlin, *Logarithmic Image Processing: Theory and Applications*, 2nd ed. Elsevier / Academic Press, 2024.

[22] A. Mittal, A. K. Moorthy, and A. C. Bovik, "No-reference image quality assessment in the spatial domain," *IEEE Transactions on Image Processing*, vol. 21, no. 12, pp. 4695–4708, 2012.

[23] A. Mittal, R. Soundararajan, and A. C. Bovik, "Making a "completely blind" image quality analyzer," *IEEE Signal Processing Letters*, vol. 20, no. 3, pp. 209–212, 2013.

[24] N. Venkatanath, D. Praneeth, M. C. Bh, S. S. Channappayya, and S. S. Medasani, "Blind image quality evaluation using perception based features," in *2015 Twenty First National Conference on Communications (NCC)*, 2015, pp. 1–6.

[25] L. Breiman, "Random forests," *Machine Learning*, vol. 45, no. 1, pp. 5–32, 2001.

[26] Y. P. Loh and C. S. Chan, "Getting to know low-light images with the exdark dataset," in *Proceedings of the IEEE/CVF Conference on Computer Vision and Pattern Recognition (CVPR) Workshops*, 2019.